Design of grazing-incidence multilayer supermirrors for hard-x-ray reflectors

Karsten D. Joensen, Peter Voutov, Andrew Szentgyorgyi, John Roll, Paul Gorenstein, Peter Høghøj, and Finn E. Christensen

Extremely broadband grazing-incidence multilayers for hard-x-ray reflection can be obtained by a gradual change of the layer thicknesses down through the structure. Existing approaches for designing similar neutron optics, called supermirrors, are shown to provide respectable performance when applied to x-ray multilayers. However, none of these approaches consider the effects of imperfect layer interfaces and absorption in the overlying layers. Adaptations of neutron designs that take these effects into account are presented, and a thorough analysis of two specific applications (a single hard-x-ray reflector and a hard-x-ray telescope) shows that an improved performance can be obtained. A multilayer whose bilayer thicknesses are given by a power law expression is found to provide the best solution; however, it is only slightly better than some of the adapted neutron designs.

Key words: Multilayer, supermirror, optimization, reflectivity, hard-x-ray optics, x-ray telescopes, synchrotron optics, plasma spectroscopy optics.

1. Introduction

Multilayers for the reflection of x rays consist of alternating layers of light and heavy materials. At each interface x rays are partially reflected, and a significant Bragg reflection occurs under circumstances in which constructive interference between the partial reflections takes place. Traditional x-ray multilayers[1] have been periodic structures in which the layer thicknesses remained constant throughout the multilayer stack. However, by a gradual change of the periodicity of the structure down through the stack, it is possible to obtain a very large continuous bandpass, with different portions of the band being reflected at different depths in the multilayer (Fig. 1).

Broadband structures were first discussed for optical films,[2] and then for multilayers intended for the reflection of thermal neutrons[3,4] and soft-x-ray gratings.[5] For soft x rays the performance is severely limited by absorption, and only a small increase in bandwidth can be obtained.[5] However, broadband neutron multilayer reflectors, termed supermirrors, have, through improvement in designs[6–8] and fabrication,[9] reached a level of performance of $>95\%$ reflectivity in a band up to three times as wide as the total reflection band, and they have become crucial components in neutron waveguides[10] and polarizers.[11]

It was recently suggested[12] that broadband x-ray multilayers might improve x-ray telescope performance above 10 keV, where the x-ray absorption is less severe. Since then, it has been theoretically and experimentally demonstrated[13–15] that the attainable x-ray reflectivity of such broadband multilayer structures is well explained by standard multilayer reflectivity theory and is large enough to be of interest as hard-x-ray optics in the fields of astrophysics, synchrotrons, and plasma spectroscopy. Even though it has been established that the x-ray reflectivities are much lower than those obtained with neutron supermirrors, the broadband x-ray multilayers are still super in that they provide reflection in bands of three to four times the width of the total reflection regime. For this reason, and in acknowledgement of their close relationship with the neutron supermirrors, we call the broadband x-ray structures x-ray supermirrors.

In spite of the similarity between neutron and x-ray supermirrors, a thorough investigation of the merits of the neutron designs, for x-ray supermirror design, has been lacking. Addressing this issue is the primary purpose of this paper. After briefly discussing

K. Joensen, P. Voutov, A. Szentgyorgyi, J. Roll, and P. Gorenstein are with the Harvard-Smithsonian Center for Astrophysics, Cambridge, Massachusetts 02138. P. Hoghoj is with the Institut Laue-Langevin, Grenoble, France. F. Christensen is with the Danish Space Research Institute, Lyngby, Denmark.

Received 31 March 1995; revised manuscript received 24 July 1995.

0003-6935/95/347935-10$06.00/0.

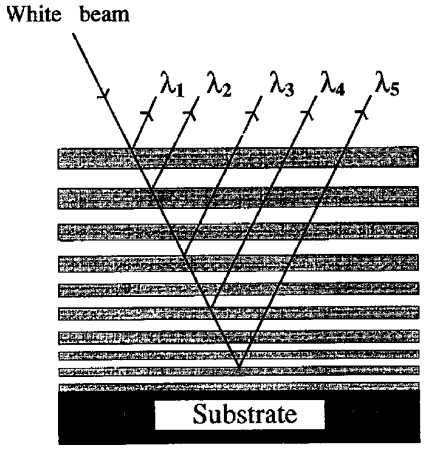

Fig. 1. Schematic illustration of the supermirror concept. The multilayer would also allow for the simultaneous reflection of a monochromatic divergent beam over a band of angles of incidence.

the model used for calculating the reflectivity of a multilayer (Section 2) and the general considerations to be taken when designing a multilayer for x-ray reflection (Section 3), we discuss the currently existing neutron designs and their performance when applied to x-ray supermirrors (Section 4). The current neutron designs do not take interface imperfections and absorption in the overlying layers into account. Both of these effects strongly influence the performance of x-ray multilayers, and it is reasonable to expect that modifications to the neutron designs will lead to improvement in the x-ray performance. In Section 5 we discuss how the neutron designs may be modified. In Sections 6 and 7 we consider the theoretical performance of the different designs for two x-ray applications: (a) a synchrotron reflector for reflection of x rays up to 70 keV and (b) a 1–100-keV x-ray Kirkpatrick–Baez astrophysics telescope. Such theoretical analysis is justified by the previously demonstrated agreement between the measured and modeled reflectivities of x-ray supermirrors.[14] Some of the modifications given in Section 5 may also prove to be applicable for neutron designs, although such a demonstration is beyond the scope of this paper.

2. Calculation of Multilayer Reflectivity

A generalized multilayer structure is seen in Fig. 2. Each layer is characterized by its location, j, in the stack, its complex refractive index, n_j, and its thickness, t_j. The complex refractive index, n, of a material with density ρ, atomic weight A, and atomic number Z is

$$n = 1 - \delta - i\beta, \tag{1}$$

where

$$\delta = \frac{\rho}{A} K f_1, \qquad \beta = \frac{\rho}{A} K f_2, \qquad K = \frac{r_e \lambda^2 N_A}{2\pi}, \tag{2}$$

r_e is the classical electron radius, λ is the wavelength,

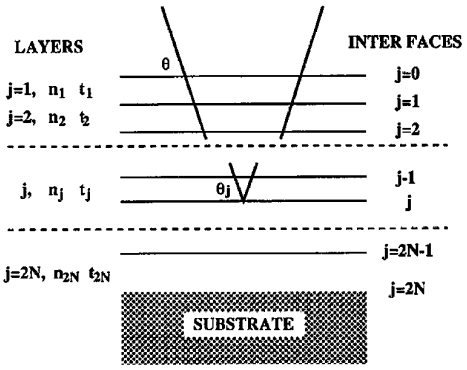

Fig. 2. Schematic illustration of the multilayer structure and the corresponding notation used in the text.

N_A is Avogadro's number, and f_1 and f_2 are the atomic scattering factors of the particular material.[16] For an ideal interface the Fresnel coefficients of reflection[17] are given by

$$r_j^s = \frac{n_j \sin\theta_j - n_{j+1} \sin\theta_{j+1}}{n_j \sin\theta_j + n_{j+1} \sin\theta_{j+1}}, \tag{3}$$

$$r_j^p = \frac{n_j \sin\theta_{j+1} - n_j \sin\theta_j}{n_j \sin\theta_{j+1} + n_{j+1} \sin\theta_j}, \tag{4}$$

where s and p refer to polarization, respectively, perpendicular and parallel to the plane of reflection, and θ_j is the internal complex angle of propagation in material j, which is most easily calculated by the use of Snell's law: $n_j \sin\theta_j = (n_j^2 - \cos^2\theta)^{1/2}$. For $\beta \ll \delta \ll 1$ (which is true for all materials in the range of energies considered here) and $\sqrt{2\delta} < \theta \ll 1$, the Fresnel coefficients both reduce to

$$r_j = \frac{2(\delta_j - \delta_{j+1})}{4 \sin^2\theta}. \tag{5}$$

The full reflectivity, R, of the multilayer is obtained by recursive use of the single-film formula[17]:

$$\chi_j = \frac{r_j + \chi_{j+1} \exp(-i2\phi_j)}{1 + r_j \chi_{j+1} \exp(-i2\phi_j)}, \tag{6}$$

$$\phi_j = \frac{2\pi}{\lambda} t_j n_j \sin\theta_j,$$

where χ_j is the reflected amplitude at the jth interface, $R = |\chi_0|^2$, and the recursion is started by the assumption that there is no reflection from the back of the substrate (i.e., $\chi_{2n+1} = 0$).

The specular reflectivity of nonideal interfaces can be calculated by multiplication of the Fresnel coefficients of reflection in Eq. (6) by a Névot–Croce roughness factor,[18]

$$F_{\mathrm{NC}} = \exp\left[-\frac{8\pi^2}{\lambda^2}(n_j \sin\theta_j)(n_{j+1} \sin\theta_{j+1})\sigma^2\right], \tag{7}$$

where σ is the rms value of the interface roughness.

This method has been experimentally found to describe the effects of interface roughness on x-ray reflectivity well.[19]

3. Designing a Multilayer for X-Ray Optics

Designing a multilayer consists of choosing materials and layer thicknesses such that the reflectivity is as high as possible for the range of angles and energies of interest. The layers usually consist of alternating layers of high- and low-density materials, whose parameters we designate h and l, respectively. High- and low-density materials are preferred because the amplitude of the interface reflection, Eq. (5), is proportional to $|\delta_h - \delta_l|$, and δ is proportional to density. For such a structure it is natural to describe the multilayer in terms of bilayers, each consisting of two adjacent layers, with bilayer thickness or d-spacing, $d_k = t_{2k-1} + t_{2k}$, of the kth bilayer. In this formalism one also defines the layer ratio, $\Gamma_k = t_{hk}/d_k$, where t_{hk} is the thickness of the heavy material.

By application of the single-film formula twice, it is found that the largest degree of constructive interference is obtained when the reflections from the top of the bilayers are in phase, i.e., $\phi_j + \phi_{j+1} = m\pi$, where m is a positive integer. This criterion can also be expressed in terms of notation from the previous section:

$$m\lambda = 2[t_j(n_j^2 - \cos^2\theta)^{1/2} + t_{j+1}(n_{j+1}^2 - \cos^2\theta)^{1/2}]. \tag{8}$$

Equation (8) is the central equation in determining the layer thicknesses that will provide reflection at particular angles and energies. For $\beta \ll \delta \ll 1$ and $\sqrt{2\delta} < \theta \ll 1$, and construct $\Gamma_k = \Gamma$, Eq. (8) becomes the well-known refraction-corrected Bragg formula[20]

$$m\lambda = 2d \sin\theta\left[1 - \frac{2(\Gamma_h\delta_h + (1 - \Gamma)\delta_l)}{\sin^2\theta}\right]^{1/2}. \tag{9}$$

For a structure of alternating materials, the largest degree of constructive interference within the bilayer is when adjacent interfaces reflect in phase. This criterion is fulfilled when $\phi_j = \pi/2$, because this leads to a phase difference of π and an additional phase shift of π is obtained at the reflection of the l–h boundary. A multilayer in which both of the criteria for maximum constructive interference are fulfilled (i.e., $\phi_j = \pi/2$ and $\phi_j + \phi_{j+1} = \pi$) is designated a quarter-wave structure.[20] This structure is ideal for multilayers with no absorption, such as many types of neutron mirrors. However, for multilayers with absorption, it is advantageous to deviate from the quarter-wave structure by having less of the heavy material, thereby decreasing the bilayer reflectivity but improving the overall transmission so that more bilayers can participate. In order to describe such general structures, we define the ratio $\gamma_k \equiv \phi_{hk}/(\phi_{hk} + \phi_{lk})$ of phase shift ϕ_{hk} in the heavy layer to the phase shift in both the heavy and the light layers. When refractive effects are disregarded, γ_k is equal to Γ_k.

4. Neutron Designs Used for X-Ray Supermirrors

Extremely broadband multilayers for the reflection of thermal neutrons were first described[3] by Mezei in 1976. The original article leaves room for some improvement in that it (a) does not include interface roughness, (b) is only valid well above the total reflection regime, and (c) is based on a kinematical approximation of the reflectivity, which does not take extinction, absorption, and multiple interface reflections into account. The original paper also contains some errors that have since been corrected.[4,6,8] In spite of these shortcomings, it demonstrated that the principle works and that extremely broad bands of reflection with very large reflectivities are achievable.

The corrected Mezei approach is included in the present analysis with a short derivation as follows: the number of bilayers, $N(k)$, in the region of the kth bilayer contributing to the Bragg reflection within a phase $\pm\alpha\pi/4$ of that of k is determined by

$$\begin{aligned}\alpha\frac{d(k)}{4} &= \sum_{l=-[N(k)/2]}^{N(k)/2} |d(k+l) - d(k)| \\ &= -\frac{\partial d(k)}{\partial k}\sum_{l=-N(k)/2}^{N(k)/2} |l| \\ &= -\frac{\partial d(k)}{\partial k}\left[\frac{N^2(k)}{4} + \frac{N(k)}{2}\right],\end{aligned} \tag{10}$$

where $d(k)$ is a monotonically decreasing function, whose value at integer values of k is the d-spacing of the kth bilayer in the multilayer, and where α simply allows one to determine the extent to which bilayers will be considered to contribute to the reflection. In Eq. (10) a second-order Taylor expansion over the number of contributing layers has been performed, but all second-order contributions cancel.

From Eq. (6) it can be found that the maximum amplitude of reflection from the kth bilayer is

$$[1 - \exp(-i2\pi\gamma_k)]\frac{2(\delta_{kh} - \delta_{kl})}{4\sin^2\theta}, \tag{11}$$

where it is assumed that $\delta \gg \beta$ and $\theta \gg \theta_c \equiv [2(\delta_{kh} - \delta_{kl})]^{1/2}$. Considering only a quarter-wave structure (i.e., $\gamma_k = 0.5$) and disregarding multiple reflections, extinction, and the fact that the $N(k)$ layers are not of the same d-spacing, one finds that the kinematical reflectivity, R, of the $N(k)$ constructively interfering bilayers is

$$R = N^2(k)\left(\frac{\delta_h - \delta_l}{\sin^2\theta}\right)^2 = \frac{N^2(k)}{4}\left[\frac{d(k)}{d_c}\right]^4, \tag{12}$$

where $d_c \equiv \lambda/(2\sin\theta_c)$. The final design can be obtained by combining Eqs. (10) and (12) and solving the resulting differential equation. This equation was later completely solved by Schelten and Mika[7] for

the case in which $R = 1$, but Mezei simplified the problem further by assuming $N \gg 1$ and $\alpha = 1$. The resulting differential equation with solution is

$$\frac{\delta d(k)}{\delta k} = -\frac{d(k)^5}{4{d_c}^4}, \tag{13}$$

$$d(k) = \frac{d_c}{k^{1/4}}, \tag{14}$$

respectively, which together with the criterion of $\gamma = 0.5$ completely describes the Mezei super mirror design.

Figure 3 shows the x-ray reflectivity of a Ni/C supermirror with 500 bilayers constructed by the use of this design. The reflectivity has been calculated with the dynamical theory given in Section 2. The rapid reflectivity oscillations for higher energies is caused by the large number of quasi-constant bilayers taking part in the reflection. In most applications these oscillations will be smoothed out as a result of the finite coherence of the incoming radiation. Such smoothing has been performed in all the following reflectivity figures. Figure 3 also shows the reflectivity [smoothed with a 1.5-keV (FWHM) Gaussian] of a multilayer with the same design, but with an interface roughness parameter of $\sigma = 5$ Å. In spite of the significant reduction that is caused by the interface roughness, the reflection band of both is still superior to that of the theoretical 300-Å gold layer, which is also included in Fig. 3.

The complete solution to the differential equation obtained by combining Eqs. (10) and (12) is

$$d(k) = \frac{R^{1/4} d_c}{\{[1 + \alpha(k + b)]^{1/2} - 1\}^{1/2}}, \tag{15}$$

with $b = a^4/\alpha + 2a^2/\alpha - 1$ and $a = R^{1/4} d_c/d(1)$. The original solution used by Schelten and Mika[7] suggests $d(1) = d_c$, $R = 1$, and $\gamma = 0.5$, with the structure completely specified by factor α. In Sections 6 and 7 it is shown that these parameter choices are not optimal.

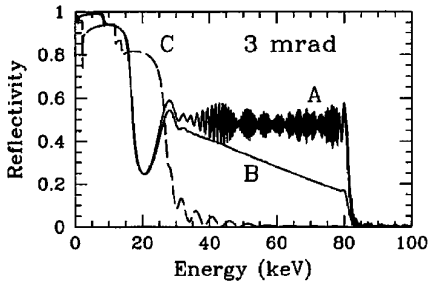

Fig. 3. Calculated reflectivity at 3 mrad of three coatings: A, a 500-bilayer Ni/C supermirror with perfect interfaces designed with the Mezei algorithm [Eq. (14)]; B, same as A but an interface roughness of $\sigma = 5.0$ Å has been included, and the reflectivity has been convoluted with a 1.5-keV (FWHM) Gaussian resolution; C, a 300-Å-thick, bulk density gold coating.

A completely different approach, explicitly incorporating the discrete nature of the multilayers, has been given by Hayter and Mook.[8] One obtains the d spacing design by recursively solving

$$\theta_k + \Delta\theta_k^- = \theta_{k-1} + \Delta\theta_{k-1}^+, \tag{16}$$

where θ_k is the angle of incidence corresponding to the kth bilayer and $\theta_k + \Delta\theta_k^-$ and $\theta_k + \Delta\theta_k^+$ are the points where the reflection amplitude from the single bilayer, k, is half that at θ_k. Even though the method works well, it is unclear how a high reflectivity was reached because the reflection from individual layers only overlaps at half-intensity, yet it is well known that above the critical edge many layers are required for high reflectivity. Recently Høghøj[21] pointed out that the reflection widths used by Hayter and Mook are a factor of $N(k)$ too small, thus in effect providing the required $N(k)$ bilayers. Nevertheless, the design is the most successful neutron design to date because of two main differences from the previous approaches: (a) extinction is explicitly taken into account by definition of $N(k)$ with the equation $1 - R = |\kappa^{N(k)}|^2$, where $|\kappa| = |(1 - r)/(1 + r)|$ is the transmission of a quarter-wave bilayer as obtained from a two-beam approximation, and (b) the recursive nature of the design allows for the explicit inclusion of refractive effects. The design is completely specified when the desired reflectivity, R, is supplied, starting with the first layer such that $3/2\sqrt{2} \times \theta_c = \theta_1 + \Delta\theta_1^-$, and when $\gamma = 0.5$ is set.

A full description of the equations that make up the Hayter and Mook approach is omitted here because they are fully described in the original article and a recent review.[22] It should be noted that the approach does not attempt to take interface roughness into account, nor are the effects of absorption on the overall performance evaluated, except as they influence refraction.

A final category of approaches is the empirical approach, in which the d-spacing structure is defined by parameters with no *a priori* physical relationships, and in which the best design is found by a search through parameter space. Such an approach was suggested by Yamada et al.[23] and consisted of the recursive use of

$$d_k = d_{k-1} - a\left(\frac{b}{d_{k-1}}\right)^{-c}, \tag{17}$$

with $b = d_1$, $a > 0$, and $\gamma = 0.5$. Another empirical design formula has been suggested by Joensen *et al.*[13] for x-ray supermirrors. The formula is a generalization of the Mezei algorithm [Eq. (14)]

$$d_k = a(b + k)^{-c}, \tag{18}$$

with $a, c > 0$ and $b > -1$. The authors obtained good results with $a \simeq 1.2 d_c$, $c \simeq 0.27$, and $b < 0$.

5. Adaptation of the Neutron Designs

The designs mentioned in Section 4 represent the core of supermirror design, but for x-ray applications they have some significant limitations. An obvious limitation is that they insist on a structure with $\gamma = 0.5$, because this is the ideal composition for nonabsorbing multilayers. However, for absorbing materials, the best performance is obtained with $\gamma < 0.5$. This is supported by the following simple calculation valid for $\theta > \theta_c$ (i.e., $\Gamma \simeq \gamma$). From formula (11) the reflectivity of a bilayer can be seen to be proportional to $(1 - \cos 2\pi\Gamma)$, and the transmission through the layers above the bilayer is proportional to $\exp[-L[\Gamma\mu_h + (1 - \Gamma)\mu_l]]$, where L is the total distance the x ray travels inside the multilayer and $\mu \equiv 4\pi\beta/\lambda$ is the material-specific linear absorption coefficient. Because for x-ray multilayers $\mu_h \gg \mu_l$, the reflectivity from this bilayer will be proportional to $(1 - \cos 2\pi\Gamma)\exp(-L\Gamma\mu_h)$, which has a maximum at

$$\Gamma = \frac{1}{2\pi} \arccos\left(\frac{L^2\mu_h{}^2 - 4\pi^2}{L^2\mu_h{}^2 + 4\pi^2}\right). \tag{19}$$

In general, $L\mu_h$ will not have the same value for all layers in the stack, so the ideal Γ will differ from layer to layer. An important exception to this is when a multilayer for polychromatic reflection at a single angle has a design similar to the power law design [Eq. (18)] with the exponent close to -0.25. In this case $L \propto E_k{}^3$ and $\mu_h \propto E_k{}^{-3}$, where E_k is the energy corresponding to the kth bilayer for the single angle under consideration. For a W/Si supermirror design that uses the power law design of Joensen *et al.* with parameters $a = 110$, $b = -0.9$, and $c = 0.25$, Eq. (19) yields an optimum $\Gamma = 0.38$. An analysis of the optimal functional form of $\gamma(k)$ is beyond the scope of this paper, and we limit the investigations to multilayers with constant Γ or γ.

Another significant limitation is that the effects of interface roughness are not considered in the designs. Roughness is very important for x rays, because the interface roughness decreases the interface reflection, necessitating the use of more layers, which in turn increases the overall absorption in the multilayer. In addition, the reduction is a function of the actual d-spacing, making it impossible to compensate by the use of parameters that influence all d spacings equally (such as R and α). However, one can easily adapt the Hayter and Mook approach to incorporate the effects of roughness by simply setting $|\kappa| = |(1 - rF_{\mathrm{NC}})/(1 + rF_{\mathrm{NC}})|$ and proceeding as previously described. The Schelten and Mika approach requires rewriting Eq. (12) to include roughness,

$$R = \frac{N^2(k)}{4}\left[\frac{d(k)}{d_c}\right]^4 \exp\left[\frac{-4\pi^2\sigma^2}{d^2(k)}\right], \tag{20}$$

and solving the differential equation obtained by combination of Eqs. (20) and (10). The solution is straightforward and is given by

$$k + b = \frac{2R d_c{}^4}{4\pi^2\sigma^2\alpha}\left(\frac{1}{d^2}(k) - \frac{1}{4\pi^2\sigma^2}\right) \times \exp\left[\frac{4\pi^2\sigma^2}{d^2(k)}\right] + \frac{4\sqrt{R}\, d_c{}^2}{4\pi^2\sigma^2\alpha}\exp\left[\frac{2\pi^2\sigma^2}{d^2(k)}\right], \tag{21}$$

where b is an integration constant whose value one finds by requiring the equation to be true for $d = d(1)$. Equation (20) can be solved for $d(k)$ by a simple Newton approach, and the structure is thus determined by α, R, $d(1)$, and choice of γ.

6. Synchrotron or Plasma-Spectroscopy Reflector

The first application we consider is a simple grazing-incidence reflector used for filtering out the high-energy component of a synchrotron spectrum[24] and suggested for filtering out the fast neutron background in plasma spectroscopy.[25] The need for hard-x-ray reflectors has risen significantly with the increased availability of hard-x-ray synchrotron sources[26] and high-temperature plasma sources.[25] Conventional high-Z-coated mirrors could fulfill this need by decreasing the grazing angle. However, this approach quickly becomes impractical because not only are the mirrors very long, but also the figure requirements become increasingly stringent. That supermirrors can reflect at higher energies than the high Z coatings makes them interesting coatings for such applications.

To evaluate the performance of the different supermirror designs, we investigate an x-ray reflector required to reflect x rays up to 70 keV, at a grazing angle of 3.5 mrad. We define the figure of merit (FOM), as the energy-weighted average reflectivity given as follows:

$$\mathrm{FOM} = \frac{\int \mathrm{d}E R(E, 3.5\ \mathrm{mrad})E}{\int \mathrm{d}E E}, \tag{22}$$

where E has been included in order to favor solutions with an enhanced response for the higher energies, and where the integral is evaluated from 0 to 70 keV.

For the analysis we have chosen to investigate a 500-bilayer W/Si supermirror with $\sigma = 4.5$ Å, because (a) W/Si supermirrors with up to 600 bilayers and total thicknesses of 1.8 μm have already been fabricated[14] and their reflectivities have been found to agree well with a modeled roughness parameter of $\sigma = 4.5$ Å, (b) the absorption edge of tungsten is located at 69.5 keV, which allows usage of the supermirror in nearly the full band of interest, and (c) W/Si multilayers have been shown to withstand intense synchrotron radiation when adequately cooled.[27] For each of the designs described in Sections 4 and 5, finding the maximum of the FOM is a classic multipa-

Table 1. Optimization Results for a 0–70 keV X-Ray Reflector with Coatings Whose *d*-Spacings Have Been Determined with the Different Designs Given in Sections 4 and 5

Model	Model No.	Structure	Parameters	FOM
Mezei	$a1$	$\gamma = 0.50$		0.3097
	$a2$	constant γ	$\gamma = 0.477$	0.3146
	$a3$	constant Γ	$\Gamma = 0.473$	0.3114
Schelten and Mika	$b1$	$\gamma = 0.5$	$R = 1.12$, $\alpha = 0.91$, $d(1) = 84$	0.3209
no roughness	$b2$	constant γ	$R = 1.41$, $\alpha = 0.98$, $d(1) = 90$, $\gamma = 0.36$	0.3354
	$b3$	constant Γ	$R = 1.32$, $\alpha = 0.8$, $d(1) = 99$, $\Gamma = 0.39$	0.3386
roughness	$c1$	$\gamma = 0.5$	$R = 0.83$, $\alpha = 1.05$, $d(1) = 96$	0.3486
	$c2$	constant γ	$R = 0.98$, $\alpha = 1.04$, $d(1) = 109.4$, $\gamma = 0.36$	0.3686
	$c3$	constant Γ	$R = 0.93$, $\alpha = 0.99$, $d(1) = 125$, $\Gamma = 0.39$	0.3697
Hayter and Mook	$d1$	$\gamma = 0.5$	$R = 0.82$	0.3197
no roughness	$d2$	constant γ	$R = 0.87$, $\gamma = 0.36$	0.3386
	$d3$	constant Γ	$R = 0.89$, $\Gamma = 0.38$	0.3449
roughness	$e1$	$\gamma = 0.5$	$R = 0.67$	0.3489
	$e2$	constant γ	$R = 0.74$, $\gamma = 0.36$	0.3731
	$e3$	constant Γ	$R = 0.75$, $\Gamma = 0.38$	0.3751
Yamada *et al.*	$f1$	$\gamma = 0.5$	$d(1) = 90$, $\Delta = 25.5$, $a = 5.73$	0.3466
	$f2$	constant γ	$d(1) = 110$, $\Delta = 45.6$, $a = 5.37$, $\gamma = 0.36$	0.3660
	$f3$	constant Γ	$d(1) = 110$, $\Delta = 41.7$, $a = 5.29$, $\Gamma = 0.40$	0.3611
Joensen *et al.*	$g1$	$\gamma = 0.5$	$a = 70$, $b = -0.918$, $c = 0.173$	0.3589
	$g2$	constant γ	$a = 81$, $b = -0.921$, $c = 0.196$, $\gamma = 0.34$	0.3823
	$g3$	constant Γ	$a = 81$, $b = -0.978$, $c = 0.193$, $\Gamma = 0.36$	0.3840

rameter optimization problem whose global solution can be sought by a variety of techniques.[28] We have chosen to use the downhill simplex algorithm, in spite of its well-known problem of terminating in local minima. We lessened the likelihood of the algorithm terminating in an undesirable local minimum by first evaluating the FOM on a grid covering a very large portion of parameter space, after which the downhill simplex was started at the best grid location. Even though the FOM is a smoothly varying function of the parameters, the exact evaluation of the FOM is difficult because, as demonstrated in Fig. 3, R is a rapidly varying function. Our experience shows that the reflectivity has to be evaluated at roughly 3000 points to achieve a 0.2% standard deviation in the FOM for points in parameter space that lie so close that they essentially should provide the same FOM.

The results of the optimizations can be seen in Table 1. The FOM is quite insensitive to the parameters near the best solution; changes in the parameters of up to 10% typically lead to a change in the FOM of only a few percent. From Table 1 it is seen that the best result is found with the Joensen *et al.* power law algorithm, closely followed by the adapted designs of Hayter and Mook and of Schelten and Mika, whereas the worst designs are those found by the use of the method of Mezei. A clear improvement is seen for those models including roughness over the corresponding models without roughness. Note that for all the different algorithms the results are best when $\gamma \neq 0.5$, but that no conclusion can be drawn as to whether a constant γ or a constant Γ is preferable. Finally, we note that the best solution ($g3$) is 20% better than the solution of the original Hayter and Mook model ($d1$), which has been claimed to be the best for neutron mirror design.[8]

Figure 4 shows the reflectivity of some of the designs. The limitations of the Mezei design are evident around the total reflection regime but are clearly improved by the original Schelten and Mika and Hayter and Mook designs. The best designs are seen to have improved performance at the harder x rays while maintaining a good low-energy performance. The Yamada *et al.* solution is seen to sacrifice some of the low-energy performance to enhance the high-energy performance. Note that the drop in reflectivity at 70 keV is due to the absorption edge of tungsten.

A deeper insight into the differences in the solution can best be obtained by closer inspection of Fig. 5, which shows the change in d-spacing from one layer to the next, normalized with respect to the corresponding d-spacing change of the Mezei design. This

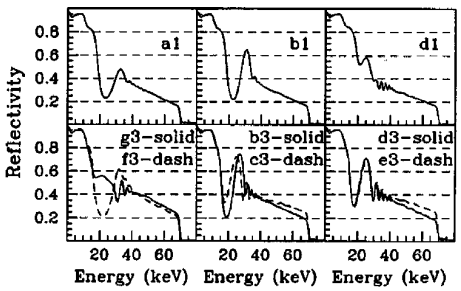

Fig. 4. Calculated reflectivities for W/Si supermirrors with roughness $\sigma = 5$ Å designed according to the models and parameters in Table 1. The curves numbered $a1$, $b1$, and $d1$ are calculated with neutron mirror designs. The other curves are calculated with the adapted or empirical designs and are seen to be superior to the neutron designs. The drop at ≈70 keV is due to the absorption edge of tungsten.

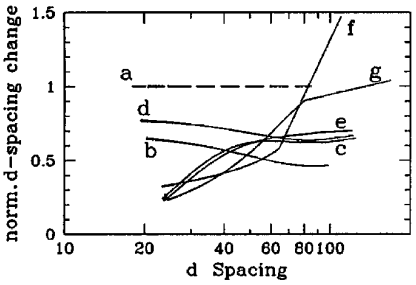

Fig. 5. Normalized d-spacing change, as defined in Eq. (23), as a function of d spacing for the best designs in each category in Table 1. The most successful designs (g, e, c, and f) are seen to change very slowly at the small d spacings, only reaching a minimum of 23 Å.

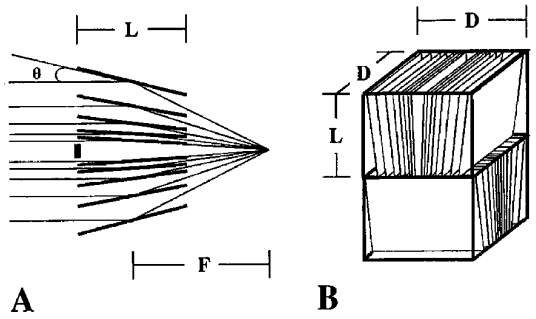

Fig. 6. Focusing scheme of a KB focusing telescope, showing one-dimensional focusing, A, and the orthogonal sets of nested reflectors making up the two-dimensional telescope, B. The dimensions are severely distorted for clarity.

quantity is defined in the following manner:

$$\frac{\Delta d(k)}{\Delta d_M(k_M)} = \frac{d(k) - d(k+1)}{d_M(k_M) - d_M(k_M+1)}, \tag{23}$$

where the subscript M refers to parameters obtained with the Mezei algorithm [Eq. (14)]. It is seen that the d-spacing change of all the solutions is for the most part smaller than that of the Mezei solution and that the most successful solutions have a relatively high rate of change at the higher d-spacings and a lower rate of change at the lower d-spacings. It is also seen that the more successful solutions have d-spacings starting near 24 Å, corresponding to a Bragg reflection at 73 keV, whereas the worse solutions have minimum d-spacings of 18–20 Å, corresponding to maximum energies of 98–90 keV, respectively. Because the integral in the FOM was evaluated only up to 70 keV, the bilayers with d-spacings of less than 24 Å do not enhance the FOM. The least successful designs cannot make use of these extra layers without degrading the performance in other regions of the band. The most successful designs are capable of decreasing the d-spacing change in the low d-spacing regime to make full usage of the 500 allotted bilayers, while keeping the number of layers in the high d-spacing regime small in order to limit absorption. Of course, the exact description of the best result would change if we were to change the expression for the FOM, by, for example, choosing another energy range, another angle, or a different number of layers. However, the above exercise clearly demonstrates that a likely application would benefit from adaptations of the original neutron designs.

7. Designing a Hard-X-Ray Kirkpatrick–Baez Telescope

The second application we consider is hard-x-ray telescopes intended for focusing x rays up to 100 keV. Several methods have been proposed to extend the present limit of x-ray telescopes to well beyond 10 keV.[29] One of these employs supermirrors on telescopes of the Wolter-I[30] geometry or the Kirkpatrick–Baez (KB) geometry.[31] We consider here the calculated on-axis performance of a KB telescope that consists of two nested sets of orthogonal paraboloid reflectors, each focusing in one dimension as illustrated in Fig. 6. We choose to evaluate the telescope performance in terms of the on-axis effective area, A, which is defined as the area of the aperture multiplied by the percentage of the radiation reaching the focus. We do not consider the effects of figure imperfections.

In a two-dimensional, grazing-incidence KB telescope, the percentage of radiation successfully focused by the first set of reflectors can be approximated by

$$P_1 = \frac{2F_1}{D}\int_0^{D/2F_1} \mathrm{d}\theta R(E, \theta)B(\theta, L, T), \tag{24}$$

where D is the distance from the outermost reflector to the optical axis, F_1 is the distance from the center of the first set of reflectors to the focal spot, and B is a weighting function that takes into account the radiation blocked by the nonzero thickness, T, of the reflectors with length L. With the assumption that there is no limit as to how closely the reflectors can be packed, B is given by $B(\theta, L, T) = \theta/(\theta + T/L)$. The percentage of radiation successfully focused from the second reflection, P_2, is calculated similarly to P_1, except that the second set of reflectors is closer to the focal point such that F_1 is substituted by $F_2 < F_1$. Total effective area A of the telescope is given by $A = 4D^2P_1P_2$.

In our present analysis we have chosen to investigate a system with $D = 3$ cm, $F_1 = 330$ cm, $F_2 = 300$ cm, $L = 30$ cm, and $T = 0.03$ cm, with a figure of merit of

$$\mathrm{FOM} = \frac{\int \mathrm{d}EA(E)E}{\int \mathrm{d}EE}, \tag{25}$$

with E included to favor solutions with an improved performance for harder x rays, and the integral evaluated from 0 to 100 keV. The FOM is essentially the energy-weighted average effective area for this 6 cm × 6 cm telescope. For this application we have chosen to investigate the performance of a

Table 2. Optimization Results for a 0–100 keV Hard X-Ray KB Telescope with Coatings in which the *d* Spacings Have Been Determined with the Methods Given in Sections 4 and 5

Model	Model No.	Structure	Parameters	FOM
Mezei	*a*1	$\gamma = 0.50$		1.788
	*a*2	constant γ	$\gamma = 0.48$	1.794
	*a*3	constant Γ	$\Gamma = 0.52$	1.728
Schelten and Mika	*b*1	$\gamma = 0.5$	$R = 1.32, \alpha = 0.91, d(1) = 184$	2.303
no roughness	*b*2	constant γ	$R = 1.33, \alpha = 0.88, d(1) = 191, \gamma = 0.41$	2.370
	*b*3	constant Γ	$R = 1.57, \alpha = 0.95, d(1) = 273, \Gamma = 0.42$	2.395
roughness	*c*1	$\gamma = 0.5$	$R = 1.05, \alpha = 1.01, d(1) = 202$	2.311
	*c*2	constant γ	$R = 1.01, \alpha = 1.13, d(1) = 214, \gamma = 0.41$	2.398
	*c*3	constant Γ	$R = 0.95, \alpha = 1.23, d(1) = 254, \Gamma = 0.42$	2.407
Hayter and Mook	*d*1	$\gamma = 0.5$	$R = 0.88$	2.309
no roughness	*d*2	constant γ	$R = 0.89, \gamma = 0.43$	2.369
	*d*3	constant Γ	$R = 0.91, \Gamma = 0.46$	2.331
roughness	*e*1	$\gamma = 0.5$	$R = 0.82$	2.281
	*e*2	constant γ	$R = 0.84, \gamma = 0.42$	2.346
	*e*3	constant Γ	$R = 0.85, \Gamma = 0.45$	2.280
Yamada *et al.*	*f*1	$\gamma = 0.5$	$d(1) = 183, \Delta = 57, a = 4.36$	2.306
	*f*2	constant γ	$d(1) = 198, \Delta = 70, a = 4.38, \gamma = 0.40$	2.394
	*f*3	constant Γ	$d(1) = 207, \Delta = 74.3, a = 4.237, \Gamma = 0.44$	2.344
Joensen *et al.*	*g*1	$\gamma = 0.5$	$a = 136, b = -0.85, c = 0.238$	2.315
	*g*2	constant γ	$a = 145, b = -0.85, c = 0.248, \gamma = 0.41$	2.444
	*g*3	constant Γ	$a = 146, b = -0.96, c = 0.246, \Gamma = 0.41$	2.471

500-bilayer Ni/C supermirror coating, because (a) neither material has absorption edges above 10 keV and (b) such multilayers have already been fabricated and their reflectivities can be modeled by the assumption of an interface roughness of $\sigma = 5$ Å.[14] We evaluated the FOM on a large grid in parameter space, evaluating the integrals at 125 angles for each of 20 energies starting at 5 keV. The downhill simplex algorithm was then started in the best grid location. The results of the optimizations can be seen in Table 2.

Once again the power law expression of Joensen *et al.* gives the best result, closely followed by the adapted designs of Schelten and Mika, Yamada *et al.*, and Hayter and Mook. It is seen that no major improvement is obtained by the use of models in which the effects of roughness are included. Allowing a structure with $\gamma \neq 0.5$ does improve performance. Figure 7 shows the effective areas of a number of these solutions, divided by the effective area of the best Mezei solution. It is seen that all the designs improve considerably on the performance of the Mezei mirror, and that the Joensen *et al.* solution (*g*3) has the best performance in the mid-energy range while maintaining a high-energy response equal to that of the other good designs. The difference between the best solution (*g*3) and the original Hayter and Mook solution (*d*1) is only 6%. Figure 8 shows the normalized *d*-spacing change as defined in Section 6 for the best solution in each of the categories. The similarities between the Schelten and Mika and the Hayter and Mook designs are seen again.

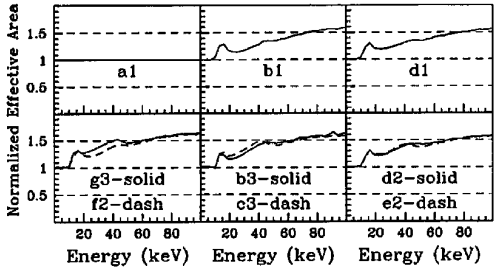

Fig. 7. Effective area for a number of the designs given in Table 2, normalized with respect to the effective area of the design obtained by the use of the Mezei algorithm. The uppermost curves are the designs obtained when the neutron algorithms are used. The lowermost are for the adapted designs and are seen to improve the performance energy range above 25 keV.

8. Discussion

This study demonstrates that neutron supermirror designs can be successfully adapted to take interface roughness explicitly into account. In addition, one can take the effects of absorption into account by allowing designs with layer ratios deviating from the quarter-wave structure. From the analysis per-

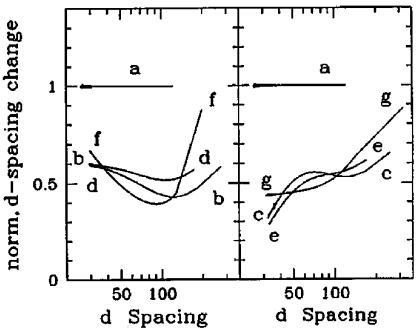

Fig. 8. Normalized d-spacing change, as defined in Eq. (23), for the best design in each category in Table 2.

formed in Sections 6 and 7, we conclude that these adaptations actually improve the performance of x-ray supermirrors. However, in both the considered applications the empirical power law description suggested by Joensen *et al.* performed better than any of the original or adapted neutron designs. We interpret this result as indicating that none of the original or adapted methods is optimal for a general application, but that the power law expression covers a larger subset of possible *d*-spacing configurations than any of the other methods and is therefore more likely to produce a structure that is close to optimal. One disadvantage of the power law equation is that the parameter space is four dimensional, making a general search considerably more time consuming than, for example, the Hayter and Mook algorithm with only a two-dimensional parameter space. It may be possible for one to improve on the multilayer design further by allowing Γ or γ to vary, and by creating more complicated empirical algorithms, but this would expand the parameter space by several additional dimensions. Solving the optimization problem completely by optimization of individual layers is probably beyond the capability of any present optimization method, because this would involve optimizing in a 1000-dimensional parameter space on a function requiring a large number of reflectivity calculations. For specific applications including several reflectors, some overall improvement of performance can also be expected if the reflectors were to be individually optimized.

A surprising result of the analysis in Sections 6 and 7 is that the performances obtained with the Hayter and Mook algorithms are no better than those obtained with the Schelten and Mika algorithms. It has previously been observed[8] that the Hayter and Mook algorithm was superior to the Schelten and Mika algorithms; however, this is not the case for x-ray supermirrors in the applications considered here. This inconsistency may be due to our present interpretation of the Schelten and Mika design that permits $d(1) \neq d_c$ and $R \neq 1$, whereas the previous comparison assumed $R = 1$ and may have assumed $d(1) = d_c$.

We note that none of the solutions found here is inherently more difficult to fabricate than any of the others, so the comparison based on the FOM is fair. The only exception to this is multilayers fabricated in systems in which the layer ratio is controlled by variation of the power to the respective targets. In this case, it is easier to deposit a multilayer with constant Γ and thereby not requiring a variation in respective target powers.

Finally, we note that broadband multilayers for x rays are primarily applicable in energy ranges in which absorption in both materials is low, such as the hard-x-ray applications considered in this paper. It is, however, also possible to envision applications in which a broad angular response is required at energies just below the absorption edge of one of the material components. One could, for example, envision a Ni/C broadband mirror with a large angular bandpass used to focus 8.05-keV CuKα. This would be possible because the absorption edge of nickel is at 8.33 keV, and absorption of 8.05-keV x rays would be small. We intend to explore these possibilities in the near future.

Major portions of this research were provided through NASA grant NAS-5138.

References

1. T. W. Barbee, Jr., "Multilayers for x-ray optics," Opt. Eng. **25,** 898–915 (1986).
2. O. S. Heavens and H. M. Liddell, "Staggered broad-band reflecting multilayers," Appl. Opt. **5,** 376–373 (1966).
3. F. Mezei, "Novel polarized neutron devices: supermirror and spin component amplifier," Commun. Phys. **1,** 81–85 (1976).
4. F. Mezei and P. A. Dagleish, "Corrigendum and first experimental evidence on neutron supermirrors," Commun. Phys. **2,** 41–43 (1977).
5. J. F. Meekins, R. G. Cruddace, and H. Gursky, "Optimization of layered synthetic microstructures for broadband reflectivity at soft x-ray and EUV wavelengths," Appl. Opt. **26,** 990–994 (1987).
6. A. G. Gukasov, V. A. Ruban, and M. N. Bedrisova, "On the feasibility of increasing the region of grazing incidence reflection of neutrons using interference in multilayers," Sov. Tech. Phys. Lett. **3,** 130–135 (1977).
7. J. Schelten and K. Mika, "Calculated reflectivities of supermirrors," Nucl. Instrum. Methods **160,** 287–294 (1979).
8. J. B. Hayter and H. A. Mook, "Discrete thin-film multilayer design for x-ray and neutron supermirrors," J. Appl. Crystallogr. **22,** 35–41 (1989).
9. J. Wood, "Status of supermirror research at OSMC," in *Neutron Optical Devices and Applications*, C. F. Majkrzak and J. L. Wood, eds., Proc. Soc. Photo-Opt. Instrum. Eng. **1738,** 22 (1992).
10. M. Rossbach, O. Schaerpf, W. Kaiser, W. Graf, A. Schirmer, W. Faber, J. Duppich, and R. Zeisler, "The use of focusing supermirror neutron guides to enhance cold neutron fluence rates," Nucl. Instrum. Methods B **35,** 181–190 (1988).
11. O. Schaerpf and N. Stuesser, "Recent progress in neutron polarizers," Nucl. Instrum. Methods A **284,** 208–211 (1989).
12. F. E. Christensen, A. Hornstrup, N. J. Westergaard, J. Schnopper, J. Wood, and K. Parker, "A graded d-spacing multilayer telescope for high-energy x-ray astronomy," in *Multilayer and Grazing Incidence X-Ray/EUV Optics*, R. B. Hoover, ed., Proc. Soc. Photo-Opt. Instrum. Eng. **1546,** 160–167 (1992).
13. K. D. Joensen, F. E. Christensen, H. W. Schnopper, P. Gorenstein, J. Susini, P. Høghøj, R. Hustache, J. Wood, and K. Parker, "Medium-sized grazing incidence high-energy x-ray telescopes employing continuously graded multilayers," in *X-Ray Detector Physics and Applications*, R. B. Hoover, ed., Proc. Soc. Photo-Opt. Instrum. Eng. **1736,** 239–248 (1992).
14. K. D. Joensen, P. Gorenstein, F. E. Christensen, P. Høghøj, E. Ziegler, J. Susini, A. Freund, D. P. Siddons, and J. Wood, "Prospects for supermirrors in hard x-ray spectroscopy," in *X-Ray and Ultraviolet Spectroscopy and Polarimetry*, S. Fineschi, ed., Proc. Soc. Photo-Opt. Instrum. Eng. **2283,** 130–139 (1994).
15. P. Høghøj, E. Ziegler, J. Susini, A. K. Freund, K. D. Joensen, and P. Gorenstein, "Broad-band focusing of hard x-rays using a supermirror," in *Physics of X-ray Multilayer Structures*, Vol. 6 of OSA 1994 Technical Digest Series (Optical Society of America, Washington, D.C., 1994), pp. 142–145.
16. B. L. Henke, "Scattering factors and mass absorption coeffi-

cients," in *X-Ray Data Booklet*, D. Vaughan, ed. (Lawrence Berkeley Laboratory, Berkeley, Calif., 1986), pp. 2.28–2.43.
17. M. Born and E. Wolf, *Principles of Optics* (Pergamon, Oxford, 1989), Chap. 1, p. 40.
18. L. Névot and P. Croce, "Caractérisation des surfaces par réflexion rasante de rayons X. Application à l'étude du polissage de quelques verres silicates," Rev. Phys. Appl. **15,** 761–779 (1980).
19. F. Stanglmeier, B. Lengeler, W. Weber, H. Göbel, and M. Schuster, "Determination of the dispersive correction f′(E) to the atomic form factor from x-ray reflection," Acta Crystallogr. Sec. A **48,** 626–639 (1992).
20. E. Spiller, *Soft-X-Ray Optics* (Society of Photo-Optical Instrumentation Engineers, Bellingham, Wash., 1994), Chap. 7, pp. 106, 114.
21. P. Høghøj, "Fabrication and characterization of W/Si multilayers," Ph.D. dissertation (University of Copenhagen, Denmark, 1995).
22. O. Schaerpf and I. S. Anderson, "The role of surfaces and interfaces in the behavior of nonpolarizing and polarizing supermirrors," Phys. B **198,** 203–212 (1994).
23. S. Yamada, T. Ebisawa, N. Achiwa, T. Akiyoshi, and S. Okamoto, "Neutron-optical properties of multilayer systems," Ann. Rep. Res. Reactor Inst. **11,** 8–27 (1978).
24. Several papers in Nucl. Instrum. Methods A **246** (1986) and A **266** (1988), and in Rev. Sci. Instrum. **60** (1988) and **63** (1992).
25. K. W. Hill, K. M. Young, S. von Goeler, H. Hsuan, R. Hulse, L.-P. Ku, B. C. Stratton, A. S. Krieger, D. Parsignault, and E. D. Franco, "ITER x-ray diagnostics studies," Rev. Sci. Instrum. **63,** 5032–5034 (1992).
26. S. S. Hasnain, J. R. Helliwell, and H. Kamitsubo, "Overview on synchrotron radiation and the need for *Journal of Synchrotron Radiation*," J. Synchrotron Rad. **1,** 1–4 (1994).
27. E. Ziegler, G. Marot, A. K. Freund, S. Joksch, H. Kawata, L. E. Berman, and M. Iarocci. Rev. Sci. Instrum. **63,** 496–500 (1992).
28. W. H. Press, B. P. Flannery, S. A. Teukolsky, and W. T. Vetterling, *Numerical Recipes: The Art of Scientific Computing* (Cambridge U. Press, London, 1986), Chap. 10, pp. 274–334.
29. P. Gorenstein and K. D. Joensen, "Focusing in the hard x-ray band," in *Proceedings of Imaging in High Energy Astronomy* (Kluwer, Amsterdam, 1995).
30. H. Wolter, "Spiegelsystem streifenden einfalls als abbildende optiken fur rontgenstrahlen," Ann. Physik. **10,** 94–114 (1952).
31. P. Kirkpatrick and A. V. Baez, "Formation of optical images by x-rays," J. Opt. Soc. Am. **38,** 766–774 (1948).